Applied Physics Letters

Enhancement of photon detection in superconducting nanowire single photon detector exposed to oscillating magnetic field

Cite as: Appl. Phys. Lett. **118**, 232603 (2021); https://doi.org/10.1063/5.0046262
Submitted: 02 February 2021 . Accepted: 24 May 2021 . Published Online: 10 June 2021

Ilan Hakimi, Naor Vardi, Amos Sharoni, Michael Rosenbluh, and Yosef Yeshurun

Enhancement of photon detection in superconducting nanowire single photon detector exposed to oscillating magnetic field

Cite as: Appl. Phys. Lett. **118**, 232603 (2021); doi: 10.1063/5.0046262
Submitted: 2 February 2021 · Accepted: 24 May 2021 ·
Published Online: 10 June 2021

Ilan Hakimi,[a] Naor Vardi, Amos Sharoni, Michael Rosenbluh, and Yosef Yeshurun

AFFILIATIONS

Department of Physics, Institute of Superconductivity and Institute for Nanotechnology, Bar-Ilan University, Ramat-Gan 5290002, Israel

[a]Author to whom correspondence should be addressed: Ilan.Hakimi@biu.ac.il

ABSTRACT

We measured the photon count rate (PCR) and dark count rate (DCR) of a superconducting nanowire single photon detector (SNSPD) exposed to either a DC magnetic field (up to 60 mT) or to a low-amplitude oscillating field (0.12–0.48 mT, up to 50 kHz). In both cases, the results show an increase in the PCR and the DCR as the DC field or the frequency of the AC field increase. However, the ratio DCR/(PCR + DCR) increases significantly with an increasing DC field, whereas this ratio is approximately constant as the frequency of the AC field increases up to frequencies in the kHz regime. The results suggest a more favorable effect of AC fields on the operation of the SNSPD.

Quantum key distribution (QKD),[1] single-photon light detection and ranging (LIDAR),[2] and telecommunication[3] are just several of the applications that have advanced in recent years due to the superconducting nanowire single photon detector (SNSPD). Known by their high system detection efficiency (SDE), low dark count rate (DCR), and high photon counting rate (PCR),[4] such detectors have become a popular research field, which aims to improve the performance and acquire better insight into the physics behind them. Research efforts turned out to be important not only for improving the device performance but also in exploring basic science, as several superconducting phenomena such as the dynamics of vortices in superconducting nanowires were tested for the first time in such superconducting nanowire device.[5]

The success of the device to detect a photon is usually ascribed to a "hot spot" created by a photon absorbed by the superconducting nanowire.[6] In equilibrium, when no illumination is carried out, the device is biased by a current I_b close to the experimental critical (switching) current $I_{c,e}$. The bias current, which flows through the device with zero resistance, results with zero voltage drop on it. Once a photon is absorbed in the superconducting nanowire, it transfers part of its energy to electrons and a hot-spot is formed. The central part of the hot-spot, which can be normal-conducting or suppressed superconducting, expels the high bias current, causing current crowding in areas where the critical current is reduced. If the absorbed photon energy is sufficient, the hot-spot expands and turns the entire cross section of the nanowire into a normal-conducting state. Further heating due to Ohmic dissipation causes the normal area to grow until the current starts to flow through the load resistance and trigger a voltage pulse. Once the energy in the superconducting nanowire is diffused, the device is reset into the superconducting state and the current returns to flow through it.

Several microscopic models have been proposed to describe the working mechanism, which enables the device to detect the absorbed photons.[7] Part of them suggest that magnetic flux lines (vortices) may also play a role in detection mechanism via vortex hoping[8] or vortex-anti-vortex nucleation.[9] Experimental works, which tested the device under a direct (DC) magnetic field, verified these assumptions and revealed an increase in both PCR and DCR.[10,11] Namely, photons, which had insufficient energy and are characterized by low DE, could now be detected by the device with higher DE.[8] However, experiments also revealed that the growth rate of the DCR is larger than the PCR growth rate,[8] increasing the ratio DCR/(PCR + DCR) and thus making impractical use of DC magnetic fields to enhance performance.[11]

The goal of this paper is to study experimentally the effect of exposing the SNSPD to a low-amplitude *oscillating* (AC) magnetic field. The idea is to manipulate AC losses,[12]

$$P \sim f^2 H_a^2, \qquad (1)$$

in order to increase the PCR. Here, P is the dissipated power, f is the frequency of the oscillating field, and H_a is the amplitude. The localized losses in the device caused by the AC field can help in expanding hot-spots with insufficient energy to develop and produce a voltage pulse. At the same time, however, the DCR can be kept low by using low amplitude magnetic fields, lower than the penetration field, B_p, for AC fields.[13] (It is important to mention that although we work below the penetration field, vortices do exist inside the sample due to spontaneous generation and high bias current.) Indeed, we find that the exposure of SNSPD to AC magnetic fields results in an increase in both DCR and PCR as the frequency increases, but at low frequencies (up to a few kHz) the ratio between them remains small, demonstrating an advantage in using AC magnetic fields.

For the fabrication of the SNSPD, a 5 nm NbN thin film was sputtered on a two-side polished 8×8 mm R-plane sapphire substrate, 430 μm thick. As shown previously (see, e.g., Ref. 14), the choice of sapphire and NbN as materials for the SNSPD yields high quality thin films, good thermal conductance,[15] and convenient fabrication process resulting in good performance of the SNSPD. Deposition of the NbN was done using DC reactive magnetron sputtering at a rate of 0.08 angstrom per second with a 99.95% pure Nb target. For achieving high quality films, the substrate was first heated to 800 °C for two hours and then cooled to 750 °C at which the sputtering took place. All this was done under a mixture of Nitrogen and Argon (10% Nitrogen) with a total pressure of 2 mTorr. The thickness of the films was verified using XRD with resulting thickness of $d = 5 \pm 1$ nm. A transition temperature of the films into the superconducting state at 12–14 K was measured using a "quantum design" physical properties measurement system (PPMS) with a sheet resistance of $\rho_{20K} = 131\ \mu\Omega \cdot \mathrm{cm}$.

The meander patterning of the SNSPD was by e-beam lithography and reactive ion etching (RIE) after a 30 nm of hydrogen silsesquioxane (HSQ) resist was spin coated on top of the NbN film. Etching was accomplished using Cl/BCl process for 40 s, ensuring that there are no remnants of NbN between the wires. After etching, a thin layer of about 15 nm of HSQ was kept on the wire for protection. Figure 1(a) exhibits an atomic force microscope (AFM) image of the device, showing a wire width $w \sim 140$ nm.

The basic PPMS was upgraded with a homemade insert, which allowed us to bring into the chamber cryogenic coax cables and a

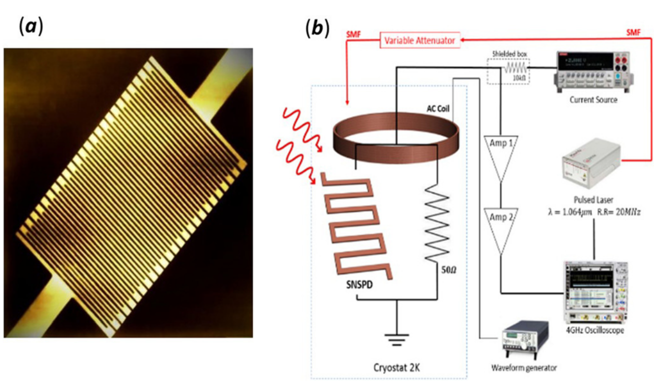

FIG. 1. (a) AFM image of the SNSPD. The device area is $10 \times 15\ \mu$m with a measured wire width of 142 and 5 nm thicknesses. (b) System schematics for SNSPD measurements.

single mode fiber (SMF). The insert also includes an alignment stage for coupling the SNSPD to the SMF, and a copper coil for producing AC magnetic field. As a light source, we used a mode-locked Toptica PicoFYb 1064 nm pulsed laser with a repetition rate of 20 MHz. The average output power of the laser (5 mW) went through a variable attenuator, which allowed attenuation of the illuminating power by 30–70 dB. The SNSPD was current biased with a Keithley 2401 source meter. The current source was connected to a shielded 10 kΩ resistor that reduced noise from the source. The SNSPD was connected in parallel with a 50 Ω resistor for the relaxation process of the device. The output signal from the device went through two amplifiers (which also served as high pass filters)—ZX60-P103LN+ (0.05–3 GHz) and ZX60-33LN+ (0.05–3 GHz) from MiniCircuits—yielding a total amplification of 33 with 0.5 dB noise. After the amplification, the signal was connected to Agilent DSO9404A 4 GHz oscilloscope that served for signal analysis and photon counting. The scope was also connected to the trigger output of the laser in order to synchronize it with the optical pulses. The synchronization helped to distinguish between photon induced pulses and dark counts. For the varying magnetic field, we used a 19 mm core, 7 mm high copper wire coil. The coil, which we placed above the SNSPD, was connected to Tabor Electronics 8023 waveform generator. The magnetic field of the coil was calibrated using a Hall-probe. In all measurements, the AC field, $\vec{H} = H_a \sin(\omega t)\hat{z}$, was applied perpendicular to the device. The measurement system is shown schematically in Fig. 1(b). All measurements were taken at $T = 2.1$ K, where we measured a reduced $T_C = 9.8$ K of the device after fabrication (probably caused by oxidation at the edges of the nanowires[16]).

First, we measured the critical current in our device: $I_{c,e} = 29.8\ \mu$A. Using typical values of NbN properties,[8] coherence length of $\xi = 4$ nm and Pearl penetration depth of $\Lambda = 60\ \mu$m, the theoretical depairing current was calculated, following Ref. 8, using a variation of the London approach, in which the Ginzburg–Landau suppression of the order parameter is taken into account: $I_{c,t} = \frac{2wI_0}{\pi e \xi} = 45.9\ \mu$A with $I_0 = c\Phi_0/(8\pi\tilde{\Lambda})$, where Φ_0 is the magnetic flux quantum, e is the Euler numer, and $\tilde{\Lambda} = \Lambda/\mu^2$ is the renormalized Pearl length caused by the supercurrent with $1 < \mu^2 < 1.157$ that describes the suppression of the order parameter. The obtained theoretical depairing current corresponds to a reduction factor $R = I_{c,e}/I_{c,t} \sim 0.65$, which is very close to the theoretical reduction factor[17] of $R_t = 0.5$ caused by the 180° turnaround in our meander. A similar value of $I_{c,e}$ was measured in Ref. 10 for a similar device.

In the following, we describe measurements of the SNSPD exposed to DC and AC magnetic fields. We start by showing the influence of DC magnetic field on our SNSPDs critical current, I_c [Fig. 2(a)]. Initially, as the field increases, a strong, approximately linear decrease in the critical current is observed (as demonstrated by the dashed line). This linear decrease is described by $I_C(H)/I_C(0) = 1 - H/H_s$,[18] where $I_C(H)$ and $I_C(0)$ are the critical currents of the device with and without magnetic field, respectively, H is the applied DC magnetic field, and $H_s = \frac{\Phi_0}{2\pi\xi W}$ is the field for entry of the first vortex. Using the parameters relevant to our sample, we obtain $H_S \cong 450$ mT, larger than the observed $H_{S,e} \cong 200$ mT. This discrepancy probably results from the meander bends, as found in Ref. 19. The obtained ratio $H_{S,e}/H_S$ is close to the reduction factor R in measured critical critical current. Above $\sim$50 mT, the decrease in I_c is

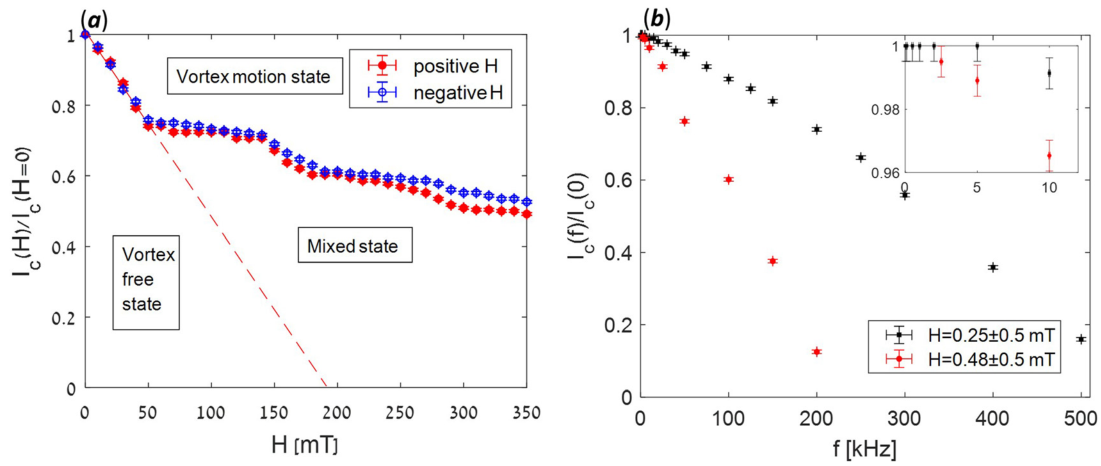

FIG. 2. (a) Critical current dependence on an external DC magnetic field. The dashed red line is a linear fit to I_c that crosses the abscicca at $H_s \sim 200$ mT. The line separates the vortex free state from the mixed state. Above I_c, loss is generated due to vortex motion. (b) The frequency dependence of the critical current (normalized to its zero field value) for AC amplitudes of 0.25 and 0.48 mT (squares and circles, respectively).

more moderate, demonstrating a crossover between a vortex-free-state (small DC fields) and the mixed state (high DC fields).[20] A similar behavior of the $I_c - H$ curve was described in a previous work,[10] with an expected value of the crossover at $H_s/2$[20] larger than 60 mT, which we obtained in our sample.

Next, we examine the device under the influence of radiation. The device was free space coupled to the SMF at distance of 3.5 mm and irradiated by 1064 nm photons. We used the lasers' external trigger that had a 5 ns duration as a synchronous signal in order to distinguish between PCR and DCR. This method was verified by obtaining similar counts of DCR for cases with and without illumination. In all the following measurements, the device was biased with a current $I_b = 0.9\, I_c(H = 0, f = 0)$. Before testing the device under the influence of magnetic fields, we verified that under this current, it operates in the regime of single photon detection by following Ref. 6 and plotting Log(PCR) vs Log(average photons per pulse) and confirming that the slope is $\sim$1. In order to be able to measure PCR enhancement, we also checked that under this bias current the device is not saturated by plotting the PCR vs the normalized bias current. As can be seen in the inset of Fig. 3, the device saturates for $I_b/I_{c,e} > 0.96$, which corresponds to a total PCR $\sim$ 3000 on average. At $0.9I_{c,e}$, the average number of PCR is $\sim$1000 s^{-1} and DCR (not shown) is $\sim$0.5 s^{-1}, which corresponds to 0.001 $s^{-1} \cdot \mu m^{-1}$ in terms of DCR per length. Although our optical setup (which allowed us to only work at 1064 nm) did not allow to gain confidence in the saturation value by examining different wavelengths, we will show later that PCR at $I = 0.9I_c$ can only be enhanced by a factor of 3, which corresponds to the saturation value we measured.

In Fig. 3, we present the effect of the magnetic field on the photon count rate [PCR(H), blue full squares, refer to the left ordinate] and the dark count rate [DCR(H), open red squares, right ordinate], normalized to their zero field values. Clearly, as the DC field increases, both the PCR and DCR grow exponentially. Taking into account both positive and negative fields, we achieve a cosh(H) dependence of the CR as predicted in Ref. 8,

$$CR_{DC} = \cosh\left(\frac{H - H_0}{H_1}\right), \tag{2}$$

where H is the external magnetic field, H_0 is an asymmetric offset, and H_1 signifies the growth rate of the exponent, which depends on the condensation energy of the hot-spot. The origin of offset field H_0 can be explained by assuming that not all turnarounds have exactly the same $I_{c,t}$.[11] This was also seen in a previous work[11] for DCR. (The authors of Ref. 11 did not see any effect of the magnetic field on the PCR so we assume that the offset was not measurable.) Fitting our data to Eq. (2), we obtain $H_{0PCR} = -7.1$ mT, $H_{0_{DCR}} = -10.9$ mT, $H_{1_{PCR}} = 25$ mT, and $H_{1_{DCR}} = 6.67$ mT. A similar behavior of an

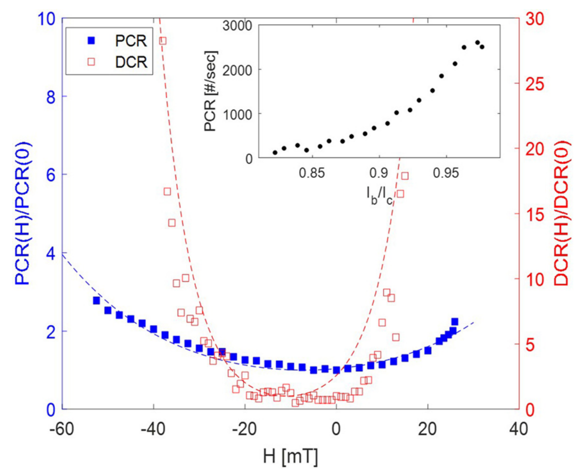

FIG. 3. The influence of a direct (DC) magnetic field on device performance at 2.1 K with I = 0.9Ic. The blue full squares describe the normalized photon count rate (left ordinate) vs DC magnetic field showing an exponential grow as the field goes high. The red open squares describe the normalized dark count rate (right ordinate). The blue and the red dashed lines are a fit to Eq. (2). Inset: Dependence of PCR on current (with $H = 0$). The device seems to saturate when $I_b/I_c > 0.96$.

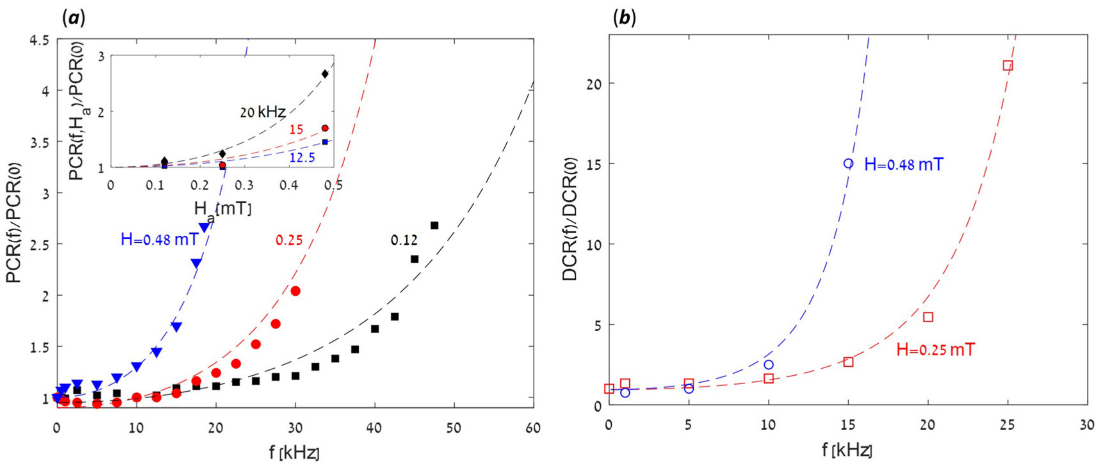

FIG. 4. (a) Alternating magnetic field influence on photon count rate as a function of the AC frequency, for fields with the indicated amplitude. The dashed lines are a fit to Eq. (3), yielding $f_0 H_{a_0} = 6.2$, 8.7, and 9.3 kHz · mT for $H_a = 0.12$, 0.25, and 0.48 mT, respectively. Inset: Amplitude dependence of the PCR for a fixed frequency. The dashed lines are fit to Eq. (3), yielding $f_0 H_{a_0} = 9.2$, 9.7, and 6.1 kHz · mT for $f = 12.5$, 15, and 20 kHz, respectively. (b) DCR under applied AC field for amplitudes of 0.25 (squares) and 0.48 mT (circles).The dashed lines are fits to Eq. (3), yielding $f_0 \cdot H_{a_0} = 3.6$ and 4.2 kHz · mT for $H_a = 0.25$ and 0.48 mT, respectively. The low DCR for 0.12 mT resulted in noisy data and is not shown in the figure.

increase in PCR and DCR under the influence of an external DC field was also observed in Refs. 10 and 21.

We continue now to describe the behavior of the SNSPD under an external AC magnetic field. In Fig. 2(b), we describe the critical current dependence on the frequency of an external AC magnetic field, for two amplitudes: 0.25 (squares) and 0.48 mT (circles). In the inset of the Fig. 2(b), we zoom on the low frequency behavior. Clearly, for low field amplitude, I_c is almost frequency independent up to ~10 kHz. Above this frequency I_c decrease slowly, vanishing (for the 0.25 mT data) at ~500 kHz. It is also apparent from the figure that an increase in the AC amplitude results in a faster decrease in the critical current. This effect of the frequency on I_c in SNSPD will be discussed and explained elsewhere.

Next, we examined the device under illumination and an external AC magnetic field. In all the measurement, the bias current I_b in the device was set to $0.9\, I_c(H = 0, f = 0)$. In Fig. 4(a), we display the influence of the AC field on the PCR (normalized to its zero field values) as a function of the frequency, f, between a few Hz and tens of kHz, for three amplitudes: $H_a = 0.12$, 0.25, and 0.48 mT (squares, circles, and triangles, respectively). In the inset of Fig. 4(a), the PCR is presented as a function of the AC amplitude H_a at fixed frequency. Based on Eq. (1), we expect the PCR to follow

$$PCR_{AC} \propto \exp\left[\left(\frac{f}{f_0}\frac{H_a}{H_{a_0}}\right)^2\right], \tag{3}$$

where $f_0 \cdot H_{a_0}$ signifies the growth rate of the exponent. The dashed lines in the figure and in the inset are fits to Eq. (3). The data show that at the low frequency range (below ~1 kHz), there is no measurable effect. We also see the influence of the AC amplitude: the larger the amplitude, the faster the PCR grows.

The influence of the AC frequency on the dark counts (normalized to their zero field values) is shown in Fig. 4(b). The results exhibit an exponential growth similar to PCR in Eq. (3). The dashed lines are fits to Eq. (3). Comparing the fitting parameters to those obtained for PCR, we see that for the same AC amplitude, DCR grows faster than PCR. The same phenomenon can be seen for the DC field in Fig. 3.

We now wish to discuss the different behavior of the device under the two different fields (DC and AC). First, we examine the performance of the device under each of the two fields separately. Both fields contribute to the improvement of PCR but also experience an increase in DCR, which can make the enhancement impractical. In Fig. 5, we plot the relative noise [DCR/(DCR + PCR)] as a function of PCR(H) normalized to its zero-field value, PCR(0). The full squares,

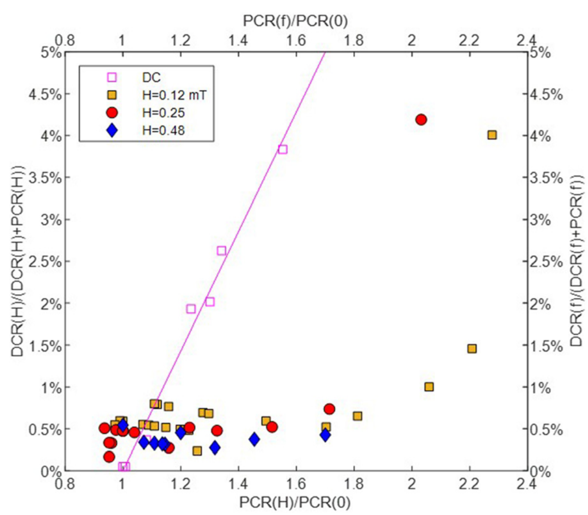

FIG. 5. Comparison between the effect of DC and AC fields at 2.1 K. The abscissa describes the growth in PCR(H) normalized to its zero-field value. The ordinate describes the ratio between DCR(H) and total counts [DCR(H)+PCR(H)]. The full squares, circles, and diamonds describe data for AC field with amplitudes of 0.12, 0.25, and 0.48 mT, respectively. The empty squares represent the measurements with DC field. The smooth line between the empty squares is a guide to the eye.

circles, and diamonds describe data for AC field with amplitudes of 0.12, 0.25, and 0.48 mT, respectively. The empty squares (with a smooth line between them as a guide to the eye) represent the measurements with DC field. The purpose of the figure is to easily examine the increase in the relative noise for each enhancement in the DE of the device. The important conclusion drawn from this figure is that for an AC field, while the PCR continues to grow, the relative noise stays around 0.5% up to PCR(f)/PCR(0) of $\sim$2. On the other hand, the DC-field relative noise grows much faster, and at around 1.1 PCR growth, it exceeds the 0.5% relative noise level. In terms of DE, if one assumes that the DE = 1 at $I_b/I_{c,e} > 0.96$ (which corresponds to $\sim$3000 s^{-1}—see the inset in Fig. 3), then at a working bias of $0.9I_{c,e}$ (which corresponds to $\sim$1000 s^{-1}) the DE is 0.3. The use of an external magnetic field can increase the DE to 0.6, while keeping the DCR as low as $\sim 0.04\,/\mathrm{s}\cdot\mu\mathrm{m}$. These data point clearly to an increase in the device performance under AC field.

An explanation to the enhancement of the PCR and DCR by DC fields was well described by two theoretical models.[8,9] Both suggest that the increased PCR and DCR are due to the introduction of magnetic flux into the device, either by vortex-crossing or vortex and anti-vortex nucleation. Since the amount of magnetic flux, which is introduced into the device using an AC field, is negligible (it is mostly due to fluctuations) compared to a DC field, we offer here a different explanation for the AC effect. We argue that the phenomenon of increased PCR and DCR due to AC field can be associated with AC losses caused by pinned vortices moving inside the pinning potential well.[22] Up to a certain magnetic field sweep rate $\dot{H}_0 = f_0 H_{a_0}$, the loss is too low to cause any detectable voltage, explaining why we hardly measured critical current reduction. Similar phenomena of critical magnetic sweep rate were observed under the research of dendritic flux avalanches.[23,24] On the other hand, this localized loss can still help the development of "weak" hot-spots caused by absorbed photons. We also believe that manipulating pinned vortices using AC loss instead of introducing more flux into sample (as in the case of DC field) is the main reason why we see in Fig. 5 that up to certain frequencies the ratio between DCR and PCR stays more or less the same, which makes the AC field more favorable. This statement is reinforced in Eq. (3), which is consistent with theoretical predictions[25,26] and experimental works[13,27] on AC losses. Since vortices exist mostly in the bends in the meander structure (where superconducting is mostly suppressed), the application of the AC field can especially help to enhance the performance of SNSPDs imagers that consist of many bended areas.[28]

To conclude, we present in this paper the study of the effect of an external AC field on the behavior of a superconducting nanowire single photon detector. A conclusive comparison was made between the effect of AC and DC field, which yields the following conclusions:

(a) The use of low-amplitude ($\sim 0.1 - 0.5\,\mathrm{mT}$) and low-frequency ($\sim 5 - 30\,\mathrm{kHz}$) AC field can help to increase PCR in a meander while keeping DCR relatively low when illuminated homogenously.
(b) The use of AC fields seems to be preferable to DC fields.
(c) Moving vortices inside their potential pinning well is most likely the origin of the enhanced performance of the SNSPD.

The present work can be a good starting point for future research in the area. In order to estimate the contribution of the effect to practical devices, further work has to be carried out. Experimentally, the reported phenomenon probably occurs at the bended areas, and therefore, it is important to study SNSPDs with other geometries or under different conditions such as with in-contact illumination that reduces the effect of the bends. Theoretically, thorough modeling of the effect of AC fields may yield a better insight into the phenomenon and help in the design of future devices.

This work was supported by the Israeli Ministry of Science and Technology (MOST), Grant No. 89055. We would also like to thank Eitan Hammami and Yosef Abulafia for their help and advice with fabrication and electronics.

DATA AVAILABILITY

The data that support the findings of this study are available from the corresponding author upon reasonable request.

REFERENCES

[1] M. K. Bhaskar, R. Riedinger, B. Machielse, D. S. Levonian, C. T. Nguyen, E. N. Knall, H. Park, D. Englund, M. Lončar, D. D. Sukachev, and M. D. Lukin, Nature **580**, 60 (2020).
[2] J. Zhu, Y. Chen, L. Zhang, X. Jia, Z. Feng, G. Wu, X. Yan, J. Zhai, Y. Wu, Q. Chen, X. Zhou, Z. Wang, C. Zhang, L. Kang, J. Chen, and P. Wu, Sci. Rep. **7**, 15113 (2017).
[3] R. H. Hadfield, Nat. Photonics **14**, 201 (2020).
[4] V. B. Verma, B. Korzh, F. Bussières, R. D. Horansky, S. D. Dyer, A. E. Lita, I. Vayshenker, F. Marsili, M. D. Shaw, H. Zbinden, R. P. Mirin, and S. W. Nam, Opt. Express **23**, 33792 (2015).
[5] A. Engel, A. D. Semenov, H.-W. Hübers, K. Il'in, and M. Siegel, Physica C **444**, 12 (2006).
[6] G. N. Gol'Tsman, O. Okunev, G. Chulkova, A. Lipatov, A. Semenov, K. Smirnov, B. Voronov, A. Dzardanov, C. Williams, and R. Sobolewski, Appl. Phys. Lett. **79**, 705 (2001).
[7] A. Engel, J. J. Renema, K. Il'in, and A. Semenov, Supercond. Sci. Technol. **28**, 114003 (2015).
[8] L. N. Bulaevskii, M. J. Graf, and V. G. Kogan, Phys. Rev. B **85**, 014505 (2012).
[9] D. Y. Vodolazov, Y. P. Korneeva, A. V. Semenov, A. A. Korneev, and G. N. Goltsman, Phys. Rev. B **92**, 104503 (2015).
[10] R. Lusche, A. Semenov, Y. Korneeva, A. Trifonov, A. Korneev, G. Gol'tsman, and H.-W. Hübers, Phys. Rev. B **89**, 104513 (2014).
[11] A. Engel, A. Schilling, K. Il'in, and M. Siegel, Phys. Rev. B **86**, 140506 (2012).
[12] E. H. Brandt, Phys. Rev. B **49**, 9024 (1994).
[13] G. P. Mikitik and E. H. Brandt, Phys. Rev. B **64**, 092502 (2001).
[14] J. A. Stern and W. H. Farr, IEEE Trans. Appl. Supercond. **17**, 306 (2007).
[15] G. A. Slack, Phys. Rev. **126**, 427 (1962).
[16] D. Henrich, S. Dörner, M. Hofherr, K. Il'in, A. Semenov, E. Heintze, M. Scheffler, M. Dressel, and M. Siegel, J. Appl. Phys. **112**, 074511 (2012).
[17] J. R. Clem, Y. Mawatari, G. R. Berdiyorov, and F. M. Peeters, Phys. Rev. B **85**, 144511 (2012).
[18] G. M. Maksimova, Phys. Solid State **40**, 1607 (1998).
[19] K. Ilin, D. Henrich, Y. Luck, Y. Liang, M. Siegel, and D. Y. Vodolazov, Phys. Rev. B **89**, 184511 (2014).
[20] G. M. Maksimova, N. V. Zhelezina, and I. L. Maksimov, Europhys. Lett. **53**, 639 (2001).
[21] A. Semenov, I. Charaev, R. Lusche, K. Ilin, M. Siegel, H.-W. Hübers, N. Bralović, K. Dopf, and D. Y. Vodolazov, Phys. Rev. B **92**, 174518 (2015).
[22] M. W. Coffey and J. R. Clem, Phys. Rev. Lett. **67**, 386 (1991).
[23] Z. Jing, H. Yong, and Y.-H. Zhou, Supercond. Sci. Technol. **28**, 075012 (2015).
[24] E. Baruch-El, M. Baziljevich, T. H. Johansen, X. Y. Zhou, X. Q. Jia, B. B. Jin, A. Shaulov, and Y. Yeshurun, Supercond. Sci. Technol. **31**, 105008 (2018).
[25] E. H. Brandt, Rep. Prog. Phys. **58**, 1465 (1995).
[26] M. W. Coffey and J. R. Clem, Phys. Rev. B **45**, 9872 (1992).
[27] A. Gurevich and G. Ciovati, Phys. Rev. B **87**, 054502 (2013).
[28] Q.-Y. Zhao, D. Zhu, N. Calandri, A. E. Dane, A. N. McCaughan, F. Bellei, H.-Z. Wang, D. F. Santavicca, and K. K. Berggren, Nat. Photonics **11**, 247 (2017).